Dynamic beam filter positioning for low-dose CT acquisition

Andrew Mao and William Shyr
Advisor: J. Webster Stayman, Ph.D

amao@jhu.edu, williamshyr@jhu.edu

A method to dynamically position x-ray beam filters for low dose CT acquisitions is needed in clinical scenarios in which accurate centering of the patient within the bore of the CT scanner is impractical. Traditional bowtie filters reduce the overall dose received by the patient without compromising image quality, but these benefits are lost when the patient is miscentered, which studies have shown results in severe image noise penalties. In some clinical imaging scenarios, such as in the emergency room (ER), the miscentering problem is overcome simply by removing the filter entirely, resulting in a large and unnecessary increase in patient dose. Our project focuses on developing a system to automatically determine the patient's position within the bore, and dynamically position the x-ray beam filter during image acquisition to confer the benefits of low-dose CT acquisitions to the emergency room. To evaluate our system's performance, we propose to perform CT acquisitions on physiological phantoms to study the relative improvements to dose and image noise using our dynamic acquisition system. This system will ultimately be applied to dynamically actuate novel beam modulators being developed by Dr. J. Web Stayman of the AIAI Laboratory to be integrated into commercial CT scanners, thus allowing beam filtering to be used for arbitrary patient positioning.

I. Project Motivation and Relevance

The great diagnostic utility of x-ray CT has led to dramatically increased use over the past decade. The associated increase in population radiation dose measurements has garnered significant public attention over the development of dose reduction methods. The number of CT procedures per year has been increasing at an annual rate $> 10\%$, and while CT represents only 15% of radiological exams using ionizing radiation, it accounts for over 50% of the effective dose [1].

Traditional CT acquisition methods have significant problems leading to increased effective dose. Existing clinical CT scanners are limited in their ability to customize data acquisitions to the patient, as CT studies are usually ordered with a "one-size fits all" mentality. Optimal data acquisition strategies vary from patient to patient and based on the anatomical site or imaging task, but the lack of any ability to create a spatially varying x-ray beam fluence profile has significant radiation dose consequences: delivering more radiation than is needed to accomplish a medical diagnosis. Because an axial slice of the patient can be seen to be ellipsoidal in shape, it is easy to see that there is less attenuating tissue at the sides of the patient than in the center. As a result, an x-ray source delivering the same beam intensity in all directions towards the patient will cause the extremities to be overexposed, which has both dose and image quality consequences. A simple solution to promote a uniform beam fluence arriving at the detector is the use of a bowtie filter, shown in Figure 1. The bowtie filter is designed simply to attenuate the beam more heavily at the sides of the patient, and can be made from a variety of materials, shown in Figure 2. A custom designed multiple aperture device (MAD), a novel beam filter developed in the AIAI laboratory, is also shown (to be discussed in more detail).

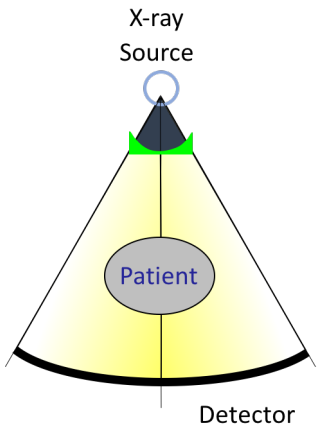

Figure 1: *Dose without bowtie translation.*

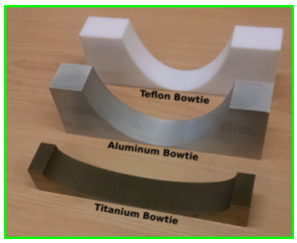

(a) *Bowties.*

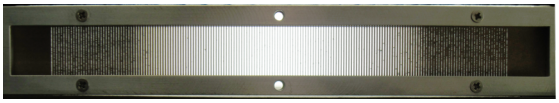

(b) *Microfabricated tungsten MAD filter.*

Figure 2: *Filters.*

While bowtie filters are commonly used in CT scanners today, they are incorporated into CT gantries spinning at fast revolutions that do not allow their translation with respect to the patient imaging plane. This creates an issue when the patient is not centered within the bore of the scanner, resulting again in the spatial misplacement of x-ray beam fluence. This scenario can result in the highly undesirable effect of increased dose in certain areas of the body, as well as increased noise in certain areas of the resulting tomograph. Habibzadeh et. al. have shown that miscentering of an average of 3 cm below the center can cause a 25.8% increase in dose and an 8.3% increase in noise [2]. Toth et. al. also showed in real clinical data that lateral positioning errors can range from -2.9 cm to 3.3 cm, and elevation errors from -6.6 to 3.4 cm, resulting in increased noise in parts of the image, shown in Figure 3 [3].

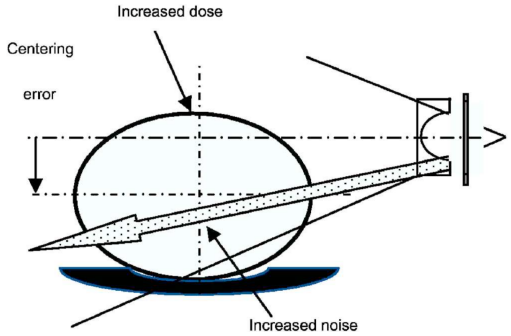

(a) *Miscentered patient.*

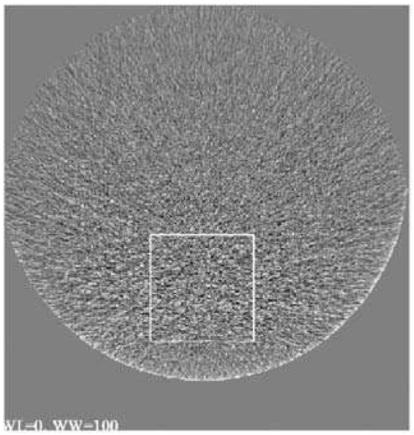

(b) *Increased noise in lower part of reconstructed image.*

Figure 3: *Miscentering.*

Clinically, centering patients within the bore is an error-strewn process that sometimes necessitates re-centering and retaking of images. While this by itself can lead to increased radiation dose, a larger need arises in imaging for emergency medicine, where time is of the essence and physicians cannot afford to spend extra time positioning the patient when making a diagnosis. Additionally, it is necessary for physicians to visualize the entire volume of the body with high image quality to make an effective diagnosis in the emergency room because there is no prior knowledge about the location of any potential disease. For these rea-

sons, it is common for the bowtie filter to be removed when imaging in the ER, resulting in increased dose and loss of the benefits of beam filtration. This scenario thus necessitates an automatic method for determining the patient's position within the bore and dynamic beam filter positioning for low-dose CT acquisitions in emergency medicine applications.

To overcome limitations preventing translation of the bowtie filters within existing clinical CT gantries, the AIAI lab has developed novel dynamic beam modulation hardware called the multiple-aperture device (MAD), described in [4, 5]. The MADs are designed to be capable of dynamically adjusting the spatial beam profile based on Moiré patterns created when two MADs are translated with respect to each other. In this project, however, we will be using only a single MAD to evaluate the efficacy of our system to avoid the extra complications associated with having two dynamic MADs. Since we will not be performing any task-based image acquisitions, the baseline profile of the single MAD will be sufficient for our experiments.

II. Technical Approach

I. Dynamic System Overview and Design

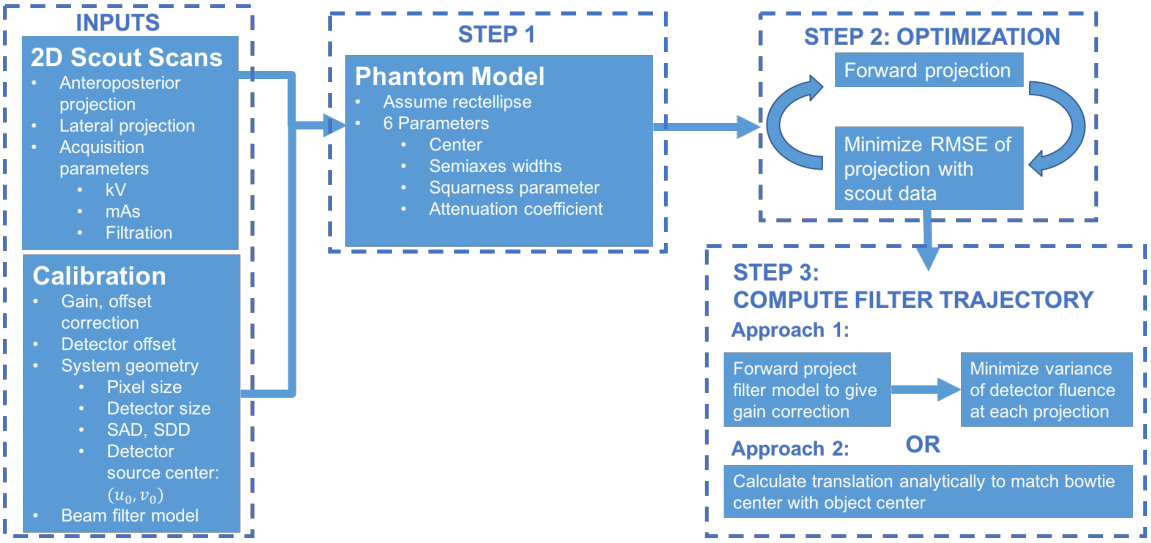

Figure 4: *Work flow of technical approach for dynamic beam positioning.*

Our system block diagram is shown in Figure 4. The patient position within the field of view is calibrated by acquiring 2D low-dose scout radiographs at two views (anteriorposterior and lateral) 90° apart, the geometry for which is shown in Figure 5. Using the estimate of the patient's position, the beam-filter trajectory over the 360° acquisition is then computed. Image acquisitions are then performed with the beam filter dynamically positioned during the acquisition arc, and images are reconstructed with the proper associated data corrections using FDK reconstruction as a baseline. All code was implemented in MATLAB, with functions for each of our different steps.

To compute the position of the phantom within the field of view (FOV) from two low-dose scout scans, simplifying assumptions about the object were made. First, only the projection data at v_0, the row corresponding to the central ray stemming from the source, is used to assume fan-beam geometry. The projection

data obtained at any view is assumed to be a function only of the position of the center of the object in the axial plane $\boldsymbol{c}_0 = (x_0, y_0)$, the width w and height h of the object in the axial plane, the gross attenuation coefficient μ and a squareness parameter of the object s. The two scout views form a data vector $\boldsymbol{g}$, and the six parameter object $\hat{\boldsymbol{x}}$ is estimated via an optimization process taking the form of

$$\hat{\boldsymbol{x}} = \arg\min_{x} \|P\boldsymbol{x} - \boldsymbol{g}\|^2 \tag{1}$$

where P is forward projection operator. The forward projector is written using standard principles for the fan-beam equi-distant geometry [6].

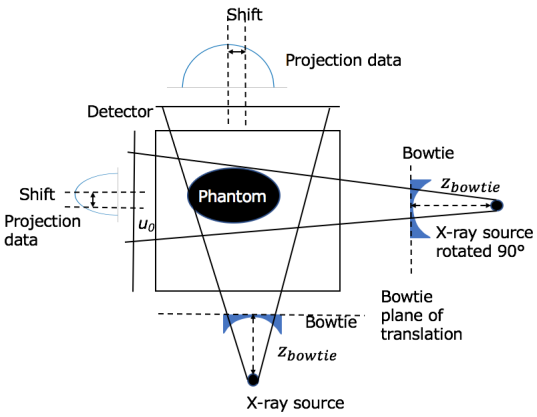

Figure 5: *Imaging geometry.*

Once the model of the phantom has been determined, an optimal beam-filter trajectory can be computed given the shape of the aluminum bowtie used and z_{bowtie}, the distance from the source to the bowtie (shown in Figure 5). z_{bowtie} is assumed to be a fixed distance from the source, which is a realistic assumption as this is unlikely to be a degree of freedom in a commercial scanner. Using these assumptions, there are two approaches to compute the beam-filter trajectory.

1. At each projection, the translation position of the bowtie producing the flattest fluence profile arriving at the detector is optimized.
2. Calculate the translation analytically to match the center of the bowtie at z_{bowtie} with the center of the phantom.

For its simplicity, we chose approach 2 for our final implementation. This was implemented by computing a θ matrix over the image of the phantom model again given by equations from [6]. However, this approach importantly required the additional assumption that the bowtie had a fixed profile that would simply shift by the specified translation distance (with magnification).

Once the beam filter trajectory is computed, the acquisition can be performed. Image reconstructions are performed using the FDK algorithm, a baseline reconstruction algorithm which simply performs filtered back-projection of cone beam CT data. This algorithm was already implemented in the CUDA Tools developed by the I-STAR Laboratory. To use FDK reconstruction, gain scans with the bowtie were also performed at each position in the trajectory to appropriately normalize and log-correct the acquisition data.

II. System Evaluation

Validation of our system's efficacy was performed using a series of experiments using both bowtie (expected deliverable) and MAD (maximum deliverable) beam filters, with and without the use of our dynamic positioning system. The cone beam CT (CBCT) test bench in the AIAI lab used for our experiments is shown in Figure 6.

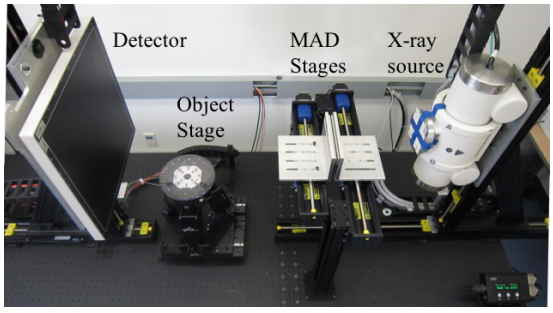

Figure 6: *CBCT Test Bench*

Image quality metrics (specifically noise) were computed on reconstructed images and dose was measured in a 16 cm diameter computed tomography dose index (CTDI) phantom. The 16cm CTDI phantom is a homogenous cylinder of PMMA intended to mimic the size of a human head and the attenuation coefficient of biological tissue, with five holes at various locations allowing for the insertion of a gas-filled ionization chamber, shown in Figure 7.

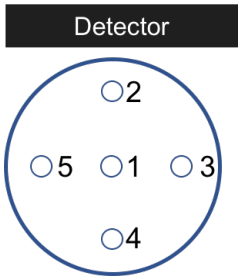

Figure 7: *16 cm PMMA CTDI Phantom.*

Accumulated dose is measured at each point, and the weighted CTDI dose is computed by

$$\begin{aligned} CTDI_w &= \frac{1}{3}CTDI_{central} + \frac{2}{3}CTDI_{peripheral} \\ &= \frac{1}{3}(d_1) + \frac{2}{3}(\frac{d_2+d_3+d_4+d_5}{4}) \end{aligned} \quad (2)$$

where

$$d_i = \text{dose at the } ith \text{ hole.}$$

In the reconstructed images, noise was analyzed in difference images of two separate scans I_1 and I_2 of the same object, according to the equation

$$\Delta I = \frac{1}{\sqrt{2}}(I_1 - I_2) \quad (3)$$

Circular ROIs were defined within the radius of the object, and an 11x11x11 box filter computing the standard deviation within the box was swept through the image to compute a "noise map." Using this noise map, contour plots demonstrating the spatial distribution of noise were then generated. The left ROI and right ROI noise was also calculated on the 11 central slices in the reconstruction.

III. Results

The positioning calibration algorithm was tested and validated on the Johnny head phantom and the 16 cm CTDI phantom, to ensure its ability to calibrate for phantoms of a variety of shapes, sizes and compositions. The fit was validated by computing RMS errors between the forward projection of the phantom model and the acquired scout data. The filter trajectory computation was verified by ensuring that the result was sinusoidal in nature, which is consistent with expectation for traditional beam filters with fixed profiles.

I. Bowtie beam filter

Figures 8a and 8b show plots of the percent dose changes relative to the perfectly centered object for the 16 cm CTDI phantom at positions of 0.0531, 1.9474, and 4.2065 cm to the left of isocenter. With a static aluminum bowtie, the dose in hole 3 increased by up to 40% at the maximum amount of miscentering, while the dose in hole 5 decreased by about the same amount. With dynamic positioning of the bowtie filter, the percent changes in dose as a function of miscentered distance are much smaller, as shown in Figure 8b. Any residual dose changes as a function of miscentering may simply be due to natural deviations associated with miscentering.

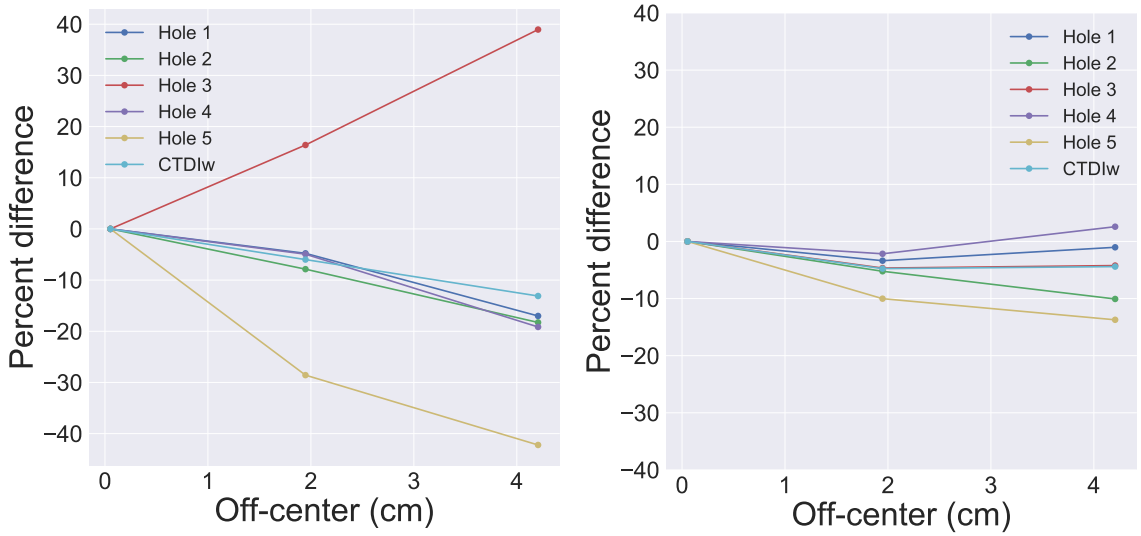

(a) *Percent change in dose with static bowtie.*

(b) *Percent change in dose with dynamic bowtie.*

Figure 8: *Dose measurements.*

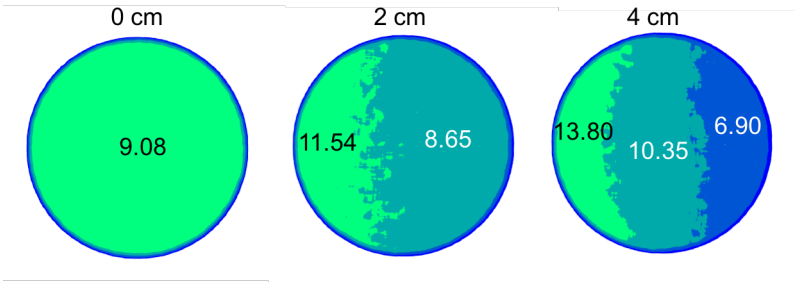

(a) *Noise distribution using static bowtie filter.*

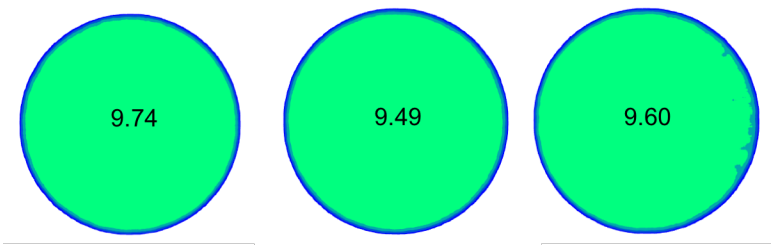

(b) *Noise distribution using dynamic bowtie filter.*

Figure 9: *Contour plots comparing noise distributions between dynamic and static bowtie filters. Noise increased with miscentering in the static case (a) and was more uniform in the dynamic case (b). All the noise magnitudes are on the order of* 10^{-4}.

Figure 9 shows the contour plots delineating the spatial distributions of noise with static and dynamic bowtie beam filters respectively. The noise distributions using dynamic beam position are almost completely uniform even with miscentering. By contrast, with a

static bowtie, the left ROI noise tends to increase while the right ROI noise tends to decrease, which corresponds to the associated decrease and increase in dose respectively. Figure 10 compares the percent changes in noise of the left and the right sides of the phantom with respect to the centered condition for both dynamic and static bowties. As expected, a greater difference in noise between the left and right ROIs is observed with the static bowtie.

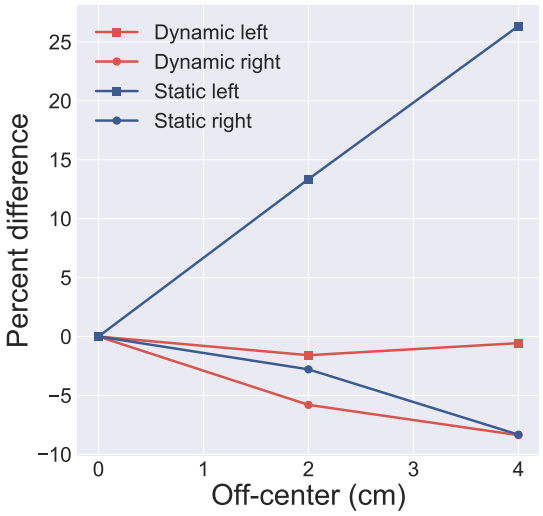

Figure 10: *Percent change in noise comparing left and right of the CTDI phantom between dynamic and static beam filters.*

II. MAD beam filter

Figures 11 and 12 show plots of the percent changes in dose for acquisitions using a single MAD filter. As expected, the dose profile trends using the single MAD filter are similar to those observed using the aluminum bowtie. Large deviations in the dose to hole numbers 3 and 5 are similarly observed with the static MAD, whereas significantly lower dose deviations as a function of miscentering distance are observed using dynamic positioning system.

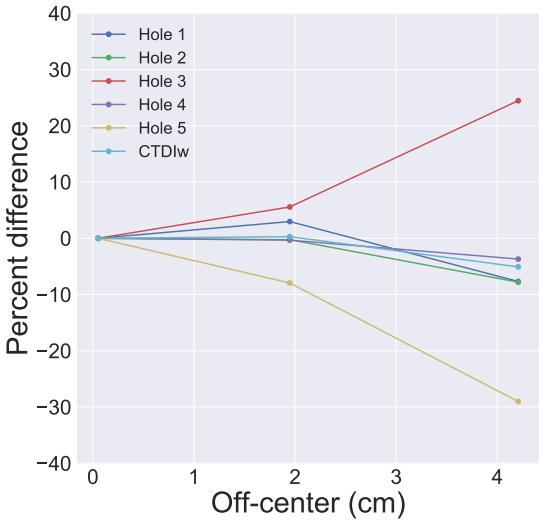

Figure 11: *Percent change in dose with static MAD.*

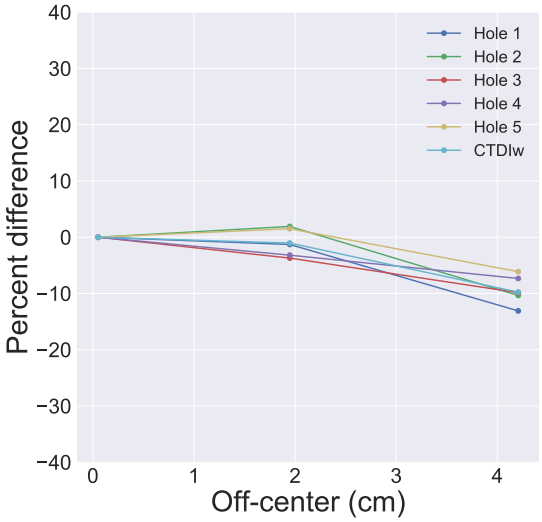

Figure 12: *Percent change in dose with dynamic MAD.*

IV. Deliverables

1. Minimum

   ☑ Constructed test bench setup and control software

   ☑ Working dose assessment and image reconstruction frameworks

   ☑ Calibration of object position in FOV using 2-view low-dose scans

☑ Computed beam filter trajectory for 360° acquisition

2. Expected

☑ Dose plots (d_i vs 3 off-center locations) for dynamic and static bowties

☑ Noise plots (σ vs 3 off-center locations) for dynamic and static bowties

3. Maximum

Noise plots (σ vs 3 off-center locations) for dynamic and static single MAD

☑ Dose plots (d_i vs 3 off-center locations) for dynamic and static single MAD

V. Dependencies

1. Technical Dependencies
   - Access to GPU workstation (Met)
   - Access to I-STAR Lab's CUDA Tools (Met)
   - Access to a variety of beam filters (Met)
   - Access to CBCT test bench (Met)
2. Advising Dependencies
   - Mentor availability (Met)

VI. Management Summary

A table outlining the division of labor for the project is shown in Figure 13.

Andrew	Will
Scout scans & filter trajectories	Phantom acquisitions
Noise assessment	Dose assessment
Test bench setup & control software	
MATLAB functions for each step of technical approach	
Version Control using Git	
Weekly Mentor Meetings	
10+ hours at JHMI per week	

Figure 13: *Management plan.*

In working on this project, we learned many skills relevant in the field of medical imaging. In particular, we learned how to use CUDA Tools, a sophisticated piece of software useful for a variety of tasks, including performing extremely speedy image reconstructions. Additionally, we learned proper protocols for characterizing dose in CT acquisitions, which is of the upmost importance in x-ray imaging.

VII. Conclusion

The aforementioned dependencies necessary for completing the project were met. The entirety of our minimum and expected deliverable were completed. However, we encountered some difficulties in the artifact correction for MAD imaging. Specifically, we were not able to fully eliminate the ring artifacts present in the reconstructed images, and were therefore unable to complete the noise analysis proposed for our maximum deliverable.

We have demonstrated that our dynamic position system works well to reduce large deviations in the dose distribution as well as promote uniform image noise for arbitrary patient positioning. However, the ultimate goal for our project is to apply our system towards acquisitions with dynamic beam filters, such as the MAD. As we have alluded to previously, the beam profile may not shift linearly with actuation distance, which we have assumed in our solution implementation. Hence, while the current system works well for traditional beam filters, it will need to be improved for dynamic and more exciting filters to truly permit fluence field modulation and achieve extremely low-dose CT.

VIII. Acknowledgements

We would like to thank the members of the AIAI lab, especially Grace Gang, Ph.D. for help making CTDI dose measurements, Steve Tilley for help with acquisitions, and our mentor Professor J. Webster Stayman, Ph.D. We would also like to thank Professor Russell Taylor, Ph.D for his advice and feedback on our presentations in class.

References

[1] S. Yousif, "Trends in examination frequency and collective effective doses from Computed Tomography (CT) procedures in Sudan", Master of Radiation and environmental protection, Sudan Academy of Sciences, 2011.

[2] Habibzadeh MA, Ay MR, Kamali AR, Ghadiri H, Zaidi H. The Influence of Patient Miscentering on Patient Dose and Image Noise in Two Commercial CT Scanners. 2010:327-330.

[3] Toth, T., Ge, Z. and Daly, M. P. (2007), The influence of patient centering on CT dose and image noise. *Med. Phys.*, 34: 3093-3101. doi:10.1118/1.2748113

[4] Stayman, J. Webster, Mathews, Aswin, Zbijewski, Wojciech, Gang, Grace J., Siewerdsen, Jeffrey H., Kawamoto Satomi, Blevis, Ira, Levinson, Reuven (2016): Fluence-field modulated x-ray CT using multiple aperture devices. In: Kontos, Despina; Flohr, Thomas; Lo, Joseph (Ed.): *SPIE Medical Imaging*, pp. 97830X, International Society for Optics and Photonics 2016.

[5] Mathews, Aswin, Tilley II, Steven, Gang, Grace J., Kawamoto, Satomi, Zbijewski, Wojciech, Siewerdsen, Jeffrey H., Levinson, Reuven, Stayman, J. Webster(2016): Design of dual multiple aperture devices for dynamical fluence field modulated CT. In: *4th International Conference on Image Formation in X-Ray Computed Tomography*, pp. 29-32, 2016.

[6] A. C. Kak and Malcolm Slaney, Principles of Computerized Tomographic Imaging, IEEE Press, 1988.

[7] Brenner DJ, Hall EJ. Computed Tomography – An Increasing Source of Radiation Exposure. 2017:2277-2284. 6. Habibzadeh MA, Ay MR, Kamali AR, Ghadiri H, Zaidi H. The Influence of Patient Miscentering on Patient Dose and Image Noise in Two Commercial CT Scanners. 2010:327-330.

[8] Pari V. Pandharipande, Andrew T. Reisner, William D. Binder, Atif Zaheer, Martin L. Gunn, Ken F. Linnau, Chad M. Miller, Laura L. Avery, Maurice S. Herring, Angela C. Tramontano, Emily C. Dowling, Hani H. Abujudeh, Jonathan D. Eisenberg, Elkan F. Halpern, Karen Donelan, and G.

Scott Gazelle. CT in the Emergency Department: A Real-Time Study of Changes in Physician Decision Making. Radiology 2016 278:3, 812-821

[9] Gies, M., Kalender, W. A., Wolf, H., Suess, C. and Madsen, M. T. (1999), Dose reduction in CT by anatomically adapted tube current modulation. I. Simulation studies. *Med. Phys.*, 26: 2235-2247. doi:10.1118/1.598779